Drying and Deposition of Picolitre Droplets of Colloidal Suspensions in Binary Solvent Mixtures

E.L. Talbot*[1] *, A. Berson*[2] *and C.D. Bain*[1] *;* [1] *Department of Chemistry, Durham University, Durham, DH1 3LE, United Kingdom;* [2] *School of Engineering and Computing Sciences, Durham University, Durham, DH1 3LE, United Kingdom

Abstract

Picolitre droplets of colloidal suspensions in a mixture of two solvents are emitted by a drop-on-demand ink jet print head onto coated and uncoated glass substrates. The evaporation rate and internal flows inside the drying droplets are investigated and the deposit pattern formed is related to the drying dynamics.

High-speed imaging of the droplet profile from the side allows the droplet diameter, height, contact angle and volume to be measured during evaporation. The internal flows throughout drying are visualized by following tracer particles within the fluid with an inverted microscope. The resulting deposits at higher solid content are imaged by scanning electron microscopy in order to relate the morphology and fine structure to the internal flows within the droplet.

The evaporation of binary solvent mixtures can cause a gradient in the surface tension at the liquid-air interface, resulting in a Marangoni flow. The ratio of solvent composition and the surface tension of the more volatile solvent relative to the less volatile solvent is varied, to manipulate the direction and magnitude of any introduced Marangoni flow. Pure solvent droplets are compared to mixed binary solvent systems, to determine the importance of Marangoni flows on the morphology of the final deposit.

Introduction

The ring deposits left after colloidal droplets dry are undesirable for ink jet printed graphics and printed electronics, where a homogeneous deposit is needed. The "coffee ring" stains develop in colloidal droplets drying with a pinned contact line [1]. Self-pinning of colloidal droplets is common, particularly for high solids content where particles wedge at the contact line preventing retraction. In order to conserve mass, a radial flow towards the contact line replenishes evaporated liquid. This convective flow transports particles inside the droplet to the periphery, building up a ring stain. One route to countering these rings is to introduce a Marangoni flow opposing the radial convective flow [2, 3].

Solvent mixtures can exhibit markedly different internal flows and evaporation behavior to their pure component fluids [4, 5]. Mixtures can be used to introduce a re-circulation flow, as preferential evaporation of the more volatile solvent causes depletion of that component at the contact line compared to the apex [7]. The resulting surface tension gradient across the free surface of the droplet causes fluid to flow from low to high surface tension. The magnitude of the Marangoni flow increases as the surface tension gradient across the liquid-vapor interface increases.

We use ethylene glycol-water and ethanol-water mixtures loaded with polystyrene spheres to determine the influence of Marangoni flows on the end deposit. A trace amount of particles is included to visualize internal flows within the droplet. The flows are then linked to the deposit structure resulting from a higher solid content using scanning electron microscopy.

Experimental

Single picolitre droplets were emitted from a drop-on-demand Microfab print head (MJ-ABP-01, Horizon Instruments), controlled by a Microfab JetDrive III Controller. The nozzle orifice was 50 μm. Fluids consisted of mixtures of ethanol-water or ethylene glycol-water filtered through a 0.45 μm pore filter. These mixtures were chosen as both ethanol and ethylene glycol have surface tensions lower than water, but ethanol is more volatile and ethylene glycol is less volatile than water (table 1). Therefore, any Marangoni flows should flow along the interface from the apex to contact line for ethanol-water and from contact line to apex for ethylene glycol-water mixtures.

Table 1. Fluid surface tensions, σ and vapor pressures, P, at 20°C [6].

Fluid	$\sigma \backslash$ mNm^{-1}	$P \backslash$ kPa
Ethanol	22.39	5.9457
Ethylene glycol	48.43	0.0074
Water	72.88	2.3374

Tracer particles of 620-nm diameter polystyrene spheres (Bangs Laboratories) were included at 0.01%v to follow internal flows. Separately, 220-nm diameter spheres (Leeds University) were added to the mixed solvents at 1%v solids, in order to view end deposits by scanning electron microscopy (SEM). Ethanol solutions with 1%v solids dried in the nozzle, so pure ethanol with 1%v solids was not printed. Consequently, in order to print ethanol-water solutions with 1%v solids, the humidity at the nozzle was raised to prevent clogging. This treatment was not needed for ethylene glycol solutions, as ethylene glycol is a humectant.

Droplets were deposited onto coated and uncoated glass substrates. Ethylene glycol mixtures were deposited onto uncoated glass and ethanol mixtures onto coated glass to increase the contact angle, improving side-on image acquisition. Glass slides were coated with silane self-assembled monolayers by vapor deposition of octadecyltrichlorosilane (OTS). The slides were first cleaned in chromic acid and rinsed with high purity water (MilliQ). Then the cleaned slides were placed in a vacuum desiccator with an open vial of OTS and the desiccator was evacuated. After 24 hours the slides were removed, rinsed in ethanol and dried in nitrogen.

Two experimental set-ups were used to capture images with

a high-speed camera (Photron APX RS) from the side and from below. To visualize internal flows, droplets were imaged from below on an inverted microscope. Droplets were illuminated from above at an angle to collect only light scattered from the particles. A 50× magnification objective (Olympus LMPLFN, NA 0.5, WD 10.6 mm) was used to magnify images. Illumination from a cold LED light source (Beaglehole Instruments) prevented uneven heating across the droplets. The ambient temperature was measured with a thermohygrometer (Extech) and was kept between 19-23°C. The relative humidity of the room was 45-50%.

Evaporation rates were determined by imaging the droplets from the side. A 20× magnification objective (Nikon MPlan, NA 0.4, WD 10 mm) was used, along with the same light source, ambient temperature and humidity. Images were post-processed in MATLAB to measure the diameter and height of the droplets by determining the total number of pixels along the droplet baseline and in the vertical direction respectively. The volume, V, and contact angle, θ, were calculated assuming a spherical cap as

$$V = \frac{\pi h}{6}\left(3R^2 + h^2\right) \tag{1}$$

and

$$\theta = 2\tan^{-1}\left(\frac{h}{R}\right), \tag{2}$$

where R is the radius of the contact area and h is the apex height. This approximation is valid for picolitre droplets which have Bond numbers, $Bo \ll 1$, so are not deformed by gravity.

Results and Discussion

Deposit Structure

SEM images of ethylene glycol-water deposits containing $1\%v$ 220-nm spheres are presented in Fig. 1.

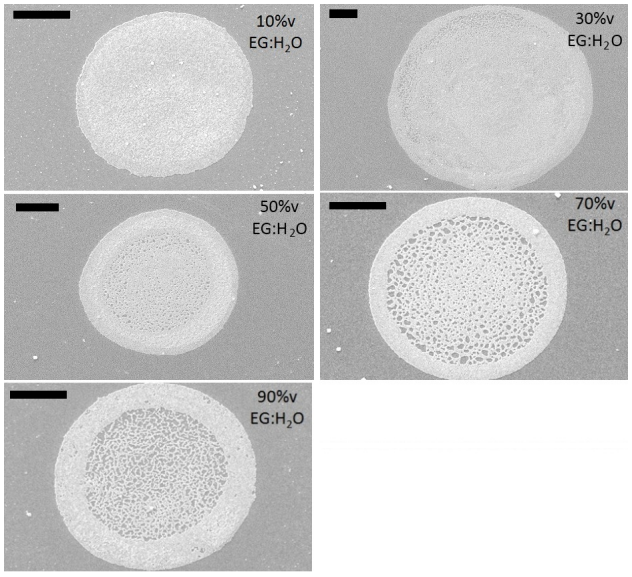

Figure 1. *Deposits from $10-90\%v$ ethylene glycol-water, containing $1\%v$ 220-nm spheres. Magnification varies and scale bars are 20 μm.*

Ring deposits were observed for $90\%v$, $70\%v$ and $50\%v$ ethylene glycol content. The $10\%v$ and $30\%v$ ethylene glycol to water ratios gave more uniform deposits, with a thicker raised edge for the $30\%v$ ratio. Deposits from pure water or ethylene glycol gave rings.

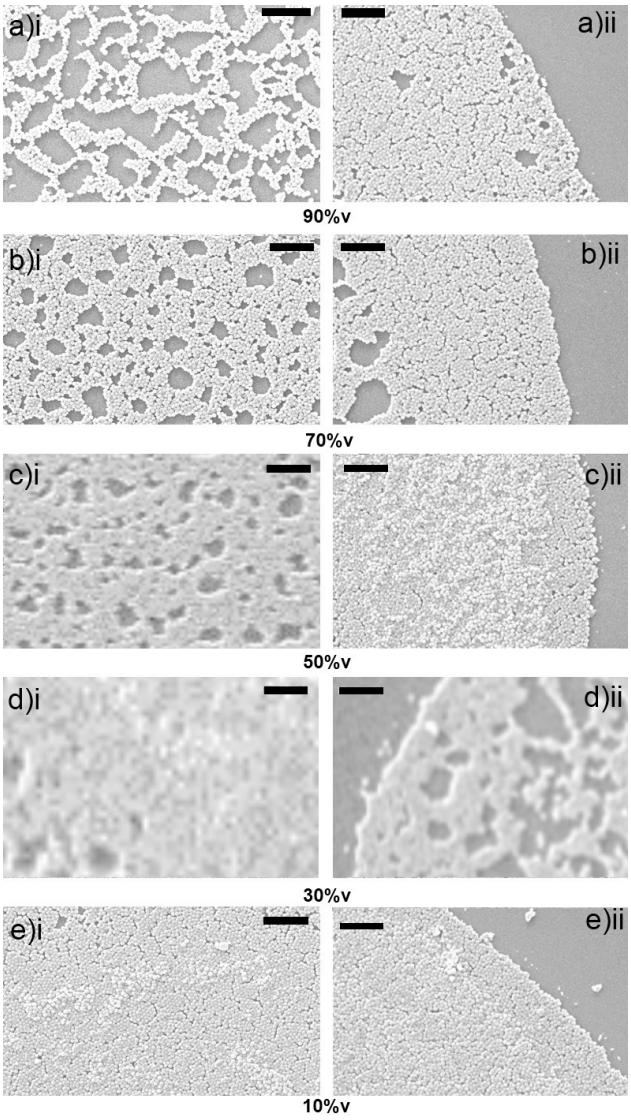

Figure 2. *Center (i) and contact line (ii) sections for a) $90\%v$, b) $70\%v$, c) $50\%v$, d) $30\%v$ and e) $10\%v$ ethylene glycol content, containing $1\%v$ 220-nm spheres. Scale bars are $2\mu m$.*

The fine structure of ethylene glycol-water deposits at the contact line and interior are compared in figure 2. The ethylene glycol-water deposits were mostly a monolayer, with a second layer starting for $10-50\%v$ ethylene glycol. The close-up of the contact line revealed that the outer edge remained a monolayer even for ethylene glycol concentrations above $50\%v$, where the droplet height at the periphery was too low for spheres to stack.

Interior packing was less dense for higher ethylene glycol content. Ratios of $50\%v$ ethylene glycol to water and above gave ring deposits, with the interior displaying unfilled regions above $70\%v$ ethylene glycol. The $10\%v$ ethylene glycol content gave

full coverage within the deposit.

Table 2 shows normalized ring widths for ethanol-water and ethylene glycol-water deposits. All ethanol concentrations gave ring deposits, with the thickest ring for 90%v ethanol compared to the deposit diameter.

Table 2. Deposit ring widths, w, normalized by the radius, R. The component volume is of ethanol or ethylene glycol (EG).

%v component	0	10	30	50	70	90	100
Ethanol, w/R	0.16	0.10	0.11	0.20	0.22	0.40	-
EG w/R	0.11	1.00	0.55	0.27	0.19	0.29	0.14

Evaporation of Mixture Components

Viewing droplets from the side showed that the initial evaporation rate was predominantly that of the more volatile component and towards the end of drying the less volatile component remained. This is consistent with the work of Sefiane [7].

The difference in evaporation rates is more obvious for ethylene glycol-water compared to ethanol-water mixtures due to the larger difference in component vapor pressures. A 50%v ethylene glycol mixture is exemplified in Fig. 3 and a 30%v in Fig. 4. There is initially a large volume loss for low ethylene glycol concentrations, with quick evaporation of mainly water, followed by a long period of ethylene glycol evaporation. Less pronounced preferential evaporation is observed for ethanol mixtures.

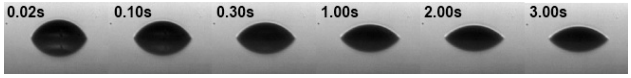

Figure 3. *An evaporating droplet of 50% ethylene glycol with no solids, at the start of drying. Initially, evaporation was mainly water with a large volume decrease until 1.86 s. Then ethylene glycol evaporation dominated until drying was complete at 232.1 s.*

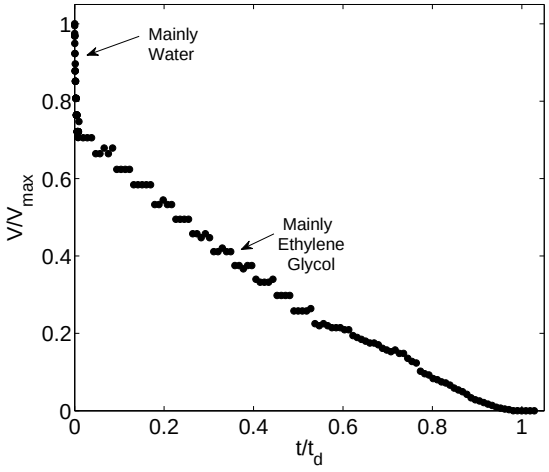

Figure 4. *Normalized volume loss with time for a 30%v ethylene glycol-water mixture, where t_d is the drying time.*

Internal Flows

By following the progression of spheres during drying, the whole picture from developing flows inside the droplet to the end resulting pattern can be traced. For pure water droplets, particle motion is radial towards the contact line following evaporation driven flow. Comparatively, ethylene glycol-water droplets initially have relatively fast particle motion radially towards the contact line due to the preferential evaporation of water. Particle motion then slows as the ethylene glycol component dominates, but motion remains radially outwards. Fig. 5 shows particle trajectories in a droplet of 10%v ethylene glycol during drying.

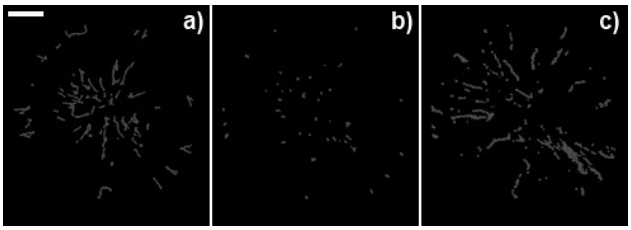

Figure 5. *Particle trajectories for 10%v ethylene glycol-water containing 0.01%v 620 nm spheres. a) Motion of particles was initially relatively fast towards the contact line (0–1 s). b) Radial motion slowed as ethylene glycol became the main component (1–2 s). c) Radial motion during remainder of drying (2 s onwards). The scale bar is 20μm.*

For high ethylene glycol content there was no evidence of Marangoni recirculation preventing radial flow to the contact line. This was expected as the corresponding deposits showed rings, and the surface tension gradient was lower at higher ethylene glycol content. Particle motion was slow and radially outwards throughout drying, particularly for 90%v ethylene glycol. For low ethylene glycol content, i.e. 10%v ethylene glycol, there was initially a faster radial flow towards the contact line. The uniform deposit at low ethylene glycol content is not fully explained by internal flows, and could be due to particles not having time to reach the contact line after the transition to ethylene glycol dominated evaporation, along with the increased solid concentration from volume loss.

The particle distribution within droplets of 50%v and 90%v ethanol is shown in Fig.s 6 and 7. The focus is just above the substrate (not all particles remain in focus throughout drying). For 10-50%v ethanol-water, the particles were initially distributed throughout the entire droplet, with motion towards and away from the contact line. As evaporation progressed (mainly ethanol), the particles became restricted to the central region. At the transition to a water droplet (with residual ethanol), particles were situated at the center. The particle motion then slowed, and radial motion to the contact line was observed due to evaporation driven flow.

For 90%v ethanol, particle velocities were slower, with circulation towards and away from the contact line. Unlike the 10-50%v cases, there was less restriction of particles to the center, and no distinct change to water dominated evaporation. The 70%v ethanol-water mixture was transitional between these two regimes, with particles initially distributed throughout the droplet and intermediate restriction to the droplet center.

For ethanol mixtures above 50%v ethanol, Marangoni flow was not strong enough to gather particles at the droplet center.

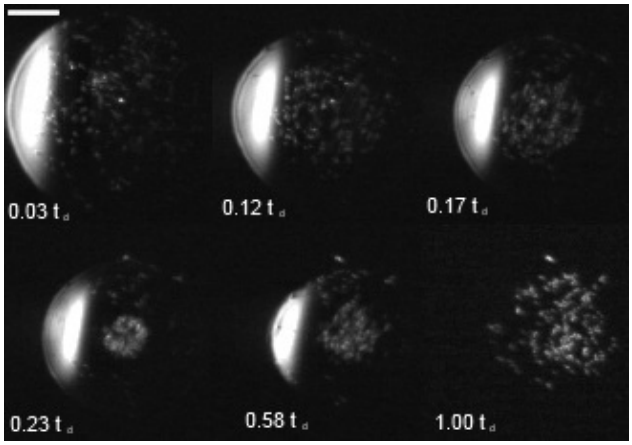

Figure 6. *Inverted microscope images for 50%v ethanol-water with 0.01%v 620-nm spheres (white). Particles were initially distributed throughout the entire droplet. As evaporation progressed particles were restricted to the center. Times are fractions of the drying time, t_d. The scale bar is 20μm.*

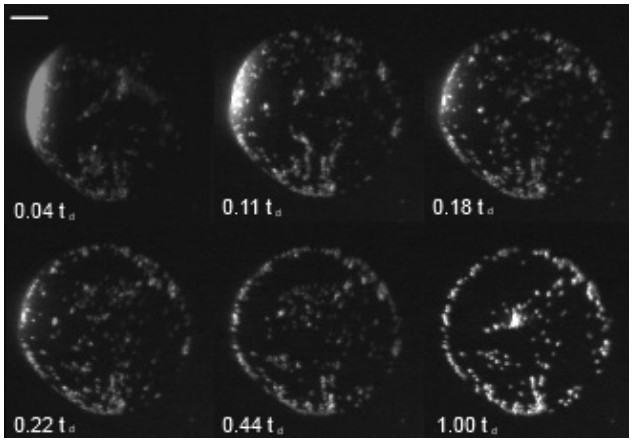

Figure 7. *Inverted microscope images for 90%v ethanol-water with 0.01%v 620-nm spheres (white). Particle motion was slower for 10%v ethanol. The particles moved towards and away from the contact line in a cycling motion. Times are given as a fraction of the drying time, t_d. The scale bar is 20μm.*

At high ethanol content (90%v), slower particle motion indicated less Marangoni recirculation than for lower ethanol content, with a ring forming in the dried droplet of 90%v ethanol containing 0.01%v 620-nm spheres. The thicker ring for the 90%v ethanol droplet containing 1%v 220-nm spheres suggests early pinning and enhancement of the ring deposit.

For mixtures of 10-50%v ethanol with 0.01%v solids, fast Marangoni flow was seen while droplets still contained ethanol. Despite the direction of Marangoni flow in ethanol droplets enhancing convection, these flows prevented particles gathering at the contact line, instead collecting particles at a central stagnation point. The combination of larger particle velocities and a higher contact angle at low ethanol content could explain why particles were not trapped at the periphery.

After the transition to the water dominated regime, particles progressed radially towards the contact line, following convective evaporation-driven flow. For lower ethanol content the water dominated regime had longer duration, hence particles had longer to reach the contact line and form a ring. Normalized ring widths for 10%v and 30%v ethanol were slightly lower than for water, suggesting a reduction of the ring due to particle motion inwards during the start of drying.

In addition, ring widths were compared relative to the solid content at the transition. It was assumed that the transition for a 30%v ethanol droplet was when the droplet volume reached 70%. At this point, the initial solid content of 1%v became 1.4%v. Exponents from a double logarithmic plot of the normalized ring width (table 2) against the solid volume fraction were 0.53$\pm$0.1 for ethanol-water and 0.78$\pm$0.1 for ethylene glycol-water. These compare within error to the exponents found for single fluid droplets [1, 8] of 0.50 for pinned droplets and 0.76 for de-pinning droplets. This suggests that while Marangoni flow can collect particles at the center, the solid volume fraction at the transition to a single component fluid determines the ring width.

Conclusion

At low ethylene glycol content (10-30%v), uniform deposits were observed, with rings forming at higher concentrations. The internal flows in ethylene glycol mixtures showed relatively fast radial progression of spheres during water dominated evaporation, and slow radial motion thereafter with no Marangoni flow. Ethanol-water deposits were all rings. Internal flows showed particle collection at the center for 10-50%v ethanol, during the initial drying phase, until water dominated evaporation gave radial progression to the contact line. At 90%v particle motion was slower, with easy pinning due to the lower contact angle, and a ring deposit formed even at low particle concentration. Comparison of the solid content once a single component fluid was reached, with the normalized ring width indicated that ring build up occurred mainly after the transition to a pure fluid.

Acknowledgments

The authors are grateful to J.P.S. Badyal for his advice on substrate fabrication and to H.N. Yow and S. Biggs (Leeds University) for providing the 220-nm spheres. This work was supported financially by EPSRC under grant number EP/H018913/1.

References

[1] R. Deegan, Phys. Rev. E **61**, 1, 475–485 (2000).
[2] H. Hu and R.G. Larson, J. Phys. Chem. B Lett. **110**, 14, 7090–7094 (2006).
[3] J. Park and J. Moon, Langmuir **22**, 8, 3506–3513 (2006).
[4] S.M. Rowan, M.I. Newton, F.W. Driewer and G. McHale, J. Phys. Chem. B **104**, 34, 8217-8220 (2000).
[5] J.R.E. Christy, K. Sefiane and E. Munro, J. Bionic Eng. **7**, 4, 321-328 (2010).
[6] Lange's Handbook of Chemistry 15th Edition, McGraw Hill (1999).
[7] K. Sefiane, L. Tadrist and M. Douglas, Int. J. Heat Mass Tran. **46**, 23, 4527-4534 (2003).
[8] Y.O. Popov, Phys. Rev. E **71**, 3, 036313 (2005).

Author Biography

Emma Talbot received her MSci Joint Honors in Chemistry and Physics from the University of Durham, UK in 2010. She then continued at the University of Durham, and is currently working towards a PhD in chemistry supervised by C.D. Bain, based on ink jet printed droplets.